Report

Current Biology

Oriented Cell Divisions Are Not Required for *Drosophila* Wing Shape

Highlights

- Loss of *mud* randomizes cell division orientation without affecting wing shape
- Loss of *mud* does not influence the orientation of growth in developing wing discs
- Cell rearrangements make a greater contribution to tissue shear in *mud* mutants
- These observations suggest wing shape may be specified by tissue-wide stresses

Authors

Zhenru Zhou, Herve Alégot, Kenneth D. Irvine

Correspondence

irvine@waksman.rutgers.edu

In Brief

Zhou et al. investigate the hypothesis that orientation of mitotic spindles plays a key role in determining organ shape. Unexpectedly, they find that orientated cell divisions are not required for the normal shape of the *Drosophila* wing and that the absence of oriented divisions can be compensated for by other cellular processes.

Zhou et al., 2019, Current Biology *29*, 1–9
March 4, 2019
https://doi.org/10.1016/j.cub.2019.01.044

CellPress

Please cite this article in press as: Zhou et al., Oriented Cell Divisions Are Not Required for *Drosophila* Wing Shape, Current Biology (2019), https://doi.org/10.1016/j.cub.2019.01.044

Current Biology
Report

Oriented Cell Divisions Are Not Required for *Drosophila* Wing Shape

Zhenru Zhou,[1] Herve Alégot,[1,2] and Kenneth D. Irvine[1,3,*]
[1]Waksman Institute and Department of Molecular Biology and Biochemistry, Rutgers University, Piscataway, NJ 08854, USA
[2]Present address: Institut de Biologie du Développement de Marseille, UMR 7288, Case 907 – Parc Scientifique de Luminy, 13288 Marseille Cedex 9, France
[3]Lead Contact
*Correspondence: irvine@waksman.rutgers.edu
https://doi.org/10.1016/j.cub.2019.01.044

SUMMARY

Formation of correctly shaped organs is vital for normal function. The *Drosophila* wing has an elongated shape, which has been attributed in part to a preferential orientation of mitotic spindles along the proximal-distal axis [1, 2]. Orientation of mitotic spindles is believed to be a fundamental morphogenetic mechanism in multicellular organisms [3–6]. A contribution of spindle orientation to wing shape was inferred from observations that mutation of Dachsous-Fat pathway genes results in both rounder wings and loss of the normal proximal-distal bias in spindle orientation [1, 2, 7]. To directly evaluate the potential contribution of spindle orientation to wing morphogenesis, we assessed the consequences of loss of the *Drosophila* NuMA homolog Mud, which interacts with the dynein complex and has a conserved role in spindle orientation [8, 9]. Loss of Mud randomizes spindle orientation but does not alter wing shape. Analysis of growth and cell dynamics in developing discs and in *ex vivo* culture suggests that the absence of oriented cell divisions is compensated for by an increased contribution of cell rearrangements to wing shape. Our results indicate that oriented cell divisions are not required for wing morphogenesis, nor are they required for the morphogenesis of other *Drosophila* appendages. Moreover, our results suggest that normal organ shape is not achieved through locally specifying and then summing up individual cell behaviors, like oriented cell division. Instead, wing shape might be specified through tissue-wide stresses that dictate an overall arrangement of cells without specifying the individual cell behaviors needed to achieve it.

RESULTS AND DISCUSSION

Loss of mud Randomizes Spindle Orientation but Does Not Alter Wing Shape

To evaluate the role of spindle orientation in directing organ shape, we examined the wings of adult flies mutant for the *Drosophila* NuMA homolog *mushroom body defect* (*mud*) [8, 9]. Flies hemizygous for an amorphic allele, mud^4, are viable and have wings that are slightly smaller, but similar in shape, to the wings of wild-type controls (Figures 1A, 1B, and 1E–1H). Similarly, adult wings from flies in which *mud* was knocked down throughout wing development by expressing a *mud* RNAi line in wing cells under *nub-Gal4* control appear similar in shape to control wings and slightly reduced in size (Figures 1C–1E and 1H; quantitation of roundness revealed no difference in males wings and only a 2% difference in female wings).

Spindle orientation is precisely controlled along two axes in the developing wing imaginal disc. Spindles are aligned parallel to the surface of the disc epithelium (perpendicular to the apical-basal axis), which ensures cell divisions occur within the plane of the disc. Spindles in most of the developing wing also tend to be oriented along the proximal distal axis, which in the central part of the disc is perpendicular to the dorsal-ventral (D-V) compartment boundary (Figures 1I–1L). It has previously been reported that *mud* mutation or RNAi disrupts the normal planar orientation of mitotic spindles in the wing disc [10, 11] and that *mud* is required for alignment of spindles induced by cell shape and tri-cellular junctions [12]. However, whether loss of *mud* also disrupts the normal proximal-distal bias in spindle orientation in the developing wing has not been reported.

To examine this, we labeled mitotic spindles by using a MiMIC insertion to create an RFP-tagged allele of the microtubule-associated protein Jupiter [13] and labeled cell junctions using a GFP-tagged E-cadherin transgene. Wing discs expressing these fluorescently labeled proteins were dissected from third-instar larvae, cultured *ex vivo*, and imaged every 6–8 min on a spinning disc confocal microscope for 12 h (Figures 1J and 1K; Videos S1 and S2). This analysis was performed using a recently developed method for *ex vivo* imaginal disc culture, which facilitates extended growth in culture and maintains disc patterning and gene expression, thus enabling dynamic imaging of cell behaviors in growing discs for an extended time [14]. The resulting videos were then segmented to identify mitotic spindles, and the final spindle orientation for dividing cells within the wing pouch was identified and measured relative to the D-V boundary (Figures 1J–1L). For spindles that were tilted toward the apical-basal axis, we used the projection of these spindles onto the XY plane. In wild-type wing discs, spindles were preferentially oriented toward the D-V boundary, consistent with earlier studies [1, 2, 7]. In contrast, in *mud* mutant wing discs or wing discs expressing a *mud* RNAi line, there was no preferred spindle

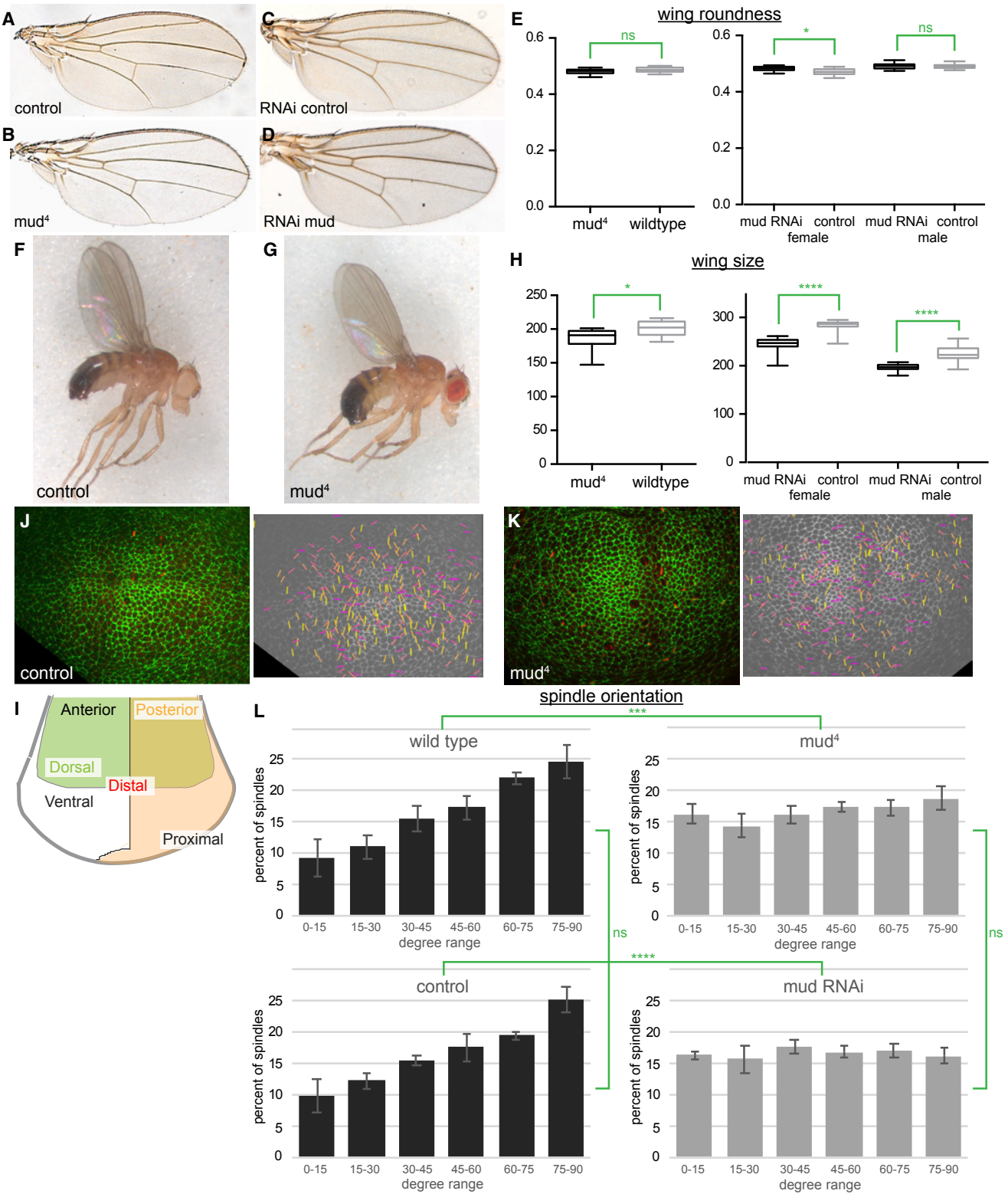

Figure 1. Loss of mud Randomizes Spindle Orientation but Does Not Alter Wing Shape

(A–D) Adult wings from (A) w^{1118}, (B) mud^4, (C) *nub-Gal4 UAS-dcr2*, and (D) *nub-Gal4 UAS-dcr2 UAS-mud-RNAi* flies.

(E) Mean roundness of wings of the indicated genotypes, calculated from 13 (mud^4), 16 (wild-type), 19 (female mud RNAi), 12 (female RNAi control), 20 (male mud RNAi), and 15 (male RNAi control) wings. Significance of differences calculated by t test is indicated.

(F and G) Adult male flies of (F) w^{1118} and (G) mud^4.

(legend continued on next page)

orientation (Figure 1L). Thus, loss of *mud* randomizes spindle orientations in the wing disc along both apical-basal [10, 11] and planar axes.

mud Mutant Wing Discs Have Oriented Growth without Oriented Cell Divisions

The observation that wing shape is normal in *mud* mutant or RNAi flies, despite randomly oriented spindles, implies that the normal orientation of cell divisions is not required for wing shape. We considered the possibility that daughter cells might reorient along the proximal-distal axis immediately after division but did not observe this in our live imaging videos. To quantitatively assess cell division orientation, we used the cell division nematics function of Tissue Analyzer software [15]. This provides an indication of the preferred cell division orientation throughout different time points of a live imaging video based on identification of daughter cells in videos with a segmented cell membrane marker. Applying this analysis to wild-type discs expressing E-cadherin:GFP revealed a preferential dorsal-ventral orientation of cell divisions, whereas applying this analysis to *mud* mutant wing discs revealed no preferred orientation of cell divisions (Figure 2A).

We also considered the possibility that compensatory mechanisms during pupal development might generate normally shaped wings despite abnormally oriented growth within the larval wing disc. To investigate the orientation of growth within discs, we used the Raeppli technique [16] to label clones of cells within developing wing discs and examined their growth. The relative elongation and orientation of labeled clones generated within *mud* RNAi discs was then compared to clones generated within control wing discs. Elongation was quantified by defining the roundness of each clone, and orientation was defined by comparing the long axis of each clone to the D-V boundary. Roundness varies from clone to clone, but the overall distribution of clone roundness within wild-type or mud RNAi wing discs is similar (Figures 2B–2D). Clones created within *mud* RNAi wing discs also tend to be oriented perpendicular to the D-V boundary, as occurs in wild-type wing discs (Figures 2B, 2C, and 2E). Thus, wing discs lacking *mud* retain oriented growth, despite lacking oriented cell divisions.

We also analyzed the overall size and shape of the wing pouch, as defined by the inner ring of Wingless (Wg) expression. Wing discs were examined at time points throughout the third larval instar (72, 84, 96, 108, and 120 h after egg laying [AEL]). Overall wing pouch size and shape were similar between wild-type and mud^4 mutant wing discs, although transient differences in size were detected around mid-third instar (Figures 2F–2I). Altogether, these observations indicate that the overall organization of growth within the developing wing disc is unaffected by the randomization of cell division orientation.

Analysis of Cell Behaviors Contributing to Wing Disc Shape

To investigate how normally oriented wing growth can occur despite abolishment of normal division orientation, we analyzed live imaging videos of wing discs expressing Jupiter:RFP and E-cad:GFP. Wing discs were dissected from mid-third-instar larvae (96 h AEL), cultured for 12–14 h, and imaged every 6–8 min throughout this time. The resulting videos were then fully segmented, including manual correction at each time point so that individual cells could be identified, characterized, and tracked. Changes in relative disc shape (shear) during culture, together with the contributions of different cell behaviors to this shape change, were analyzed using the TissueMiner computational framework [17]. A key component of this approach involves triangulation of segmented cellular networks to identify and quantify the contributions of different types of cell behaviors to tissue shear [17, 18] (Figure 3A).

In the coordinate system used to measure shear, positive shear indicates shear parallel to the wing D-V boundary, whereas negative shear indicates shear perpendicular to the D-V boundary (Figure 3B). Analysis of the wing pouch regions of three wild-type wing discs revealed an accumulation of negative shear over time, indicating that shear perpendicular to the D-V boundary occurs. Analysis of cell dynamics revealed that three cell behaviors account for most of this shear: oriented cell divisions; T1 transitions (cell rearrangements); and cell elongation (Figure 3C). The respective contributions of these different cellular processes vary from disc to disc. The results of our analysis are similar to those of Dye et al. [14], who developed the methods for long-term disc culture and analysis that we used, both in terms of the total shear detected and the contributions of different cellular processes to this shear.

We performed the same analysis on five *mud* mutant wing discs. As in wild-type, *mud* mutant discs proliferated throughout 12 h of *ex vivo* culture, although, on average, fewer cell divisions were detected (Figure S1A). Direct observation revealed that, in a fraction of cell divisions (~15%), a spindle orientation perpendicular to the plane of the disc epithelium results in the basal extrusion of one of the daughter cells. In most cases, these extruded daughter cells are permanently lost and apoptotic cells can be detected basal to the disc epithelium of *mud* mutant discs (Figure S1C), although, in a few cases (9% of these perpendicular divisions), the more basal cell later re-enters the disc epithelium. As in wild-type, *mud* mutant wings cultured *ex vivo* undergo a negative shear that accumulates over time (Figures

(H) Mean wing area (in a.u.) for the indicated genotypes. Significance of differences calculated by t test is indicated.

(I) Schematic of the wing disc showing the anterior-posterior (AP), dorsal-ventral (DV), and distal-proximal (PD) regions.

(J and K) Snapshots from *ex vivo* live imaging of control (J) or mud^4 (K) wing discs, with cell junctions labeled by E-cadherin:GFP and spindles labeled by Jupiter:RFP. In images at right, all spindle orientations from a 14-h video are plotted onto one image. Each line represents one spindle. Yellow identifies spindles perpendicular (60°–90°), orange identifies spindles 30°–60°, and magenta identifies spindles parallel (0°–30°) to the D-V boundary.

(L) Quantitative analyses of spindle orientation with respect to the D-V boundary in cultured wing discs from *wild-type control* (w^{1118}; N = 1,797 spindles from 5 discs), mud^4 (N = 1,722 spindles from 5 discs), *nub-Gal4 UAS-dcr2* control (N = 643 spindles from 3 discs), and *nub-Gal4 UASdcr2 UAS-mud-RNAi* (N = 1,088 spindles from 3 discs).

Error bars show the SD in results from different discs. The results of chi-square tests of comparisons of the distributions are indicated in green. ns, $P > 0.05$; * $P \leq 0.05$; *** $P \leq 0.001$; **** $P \leq 0.0001$. See also Videos S1 and S2.

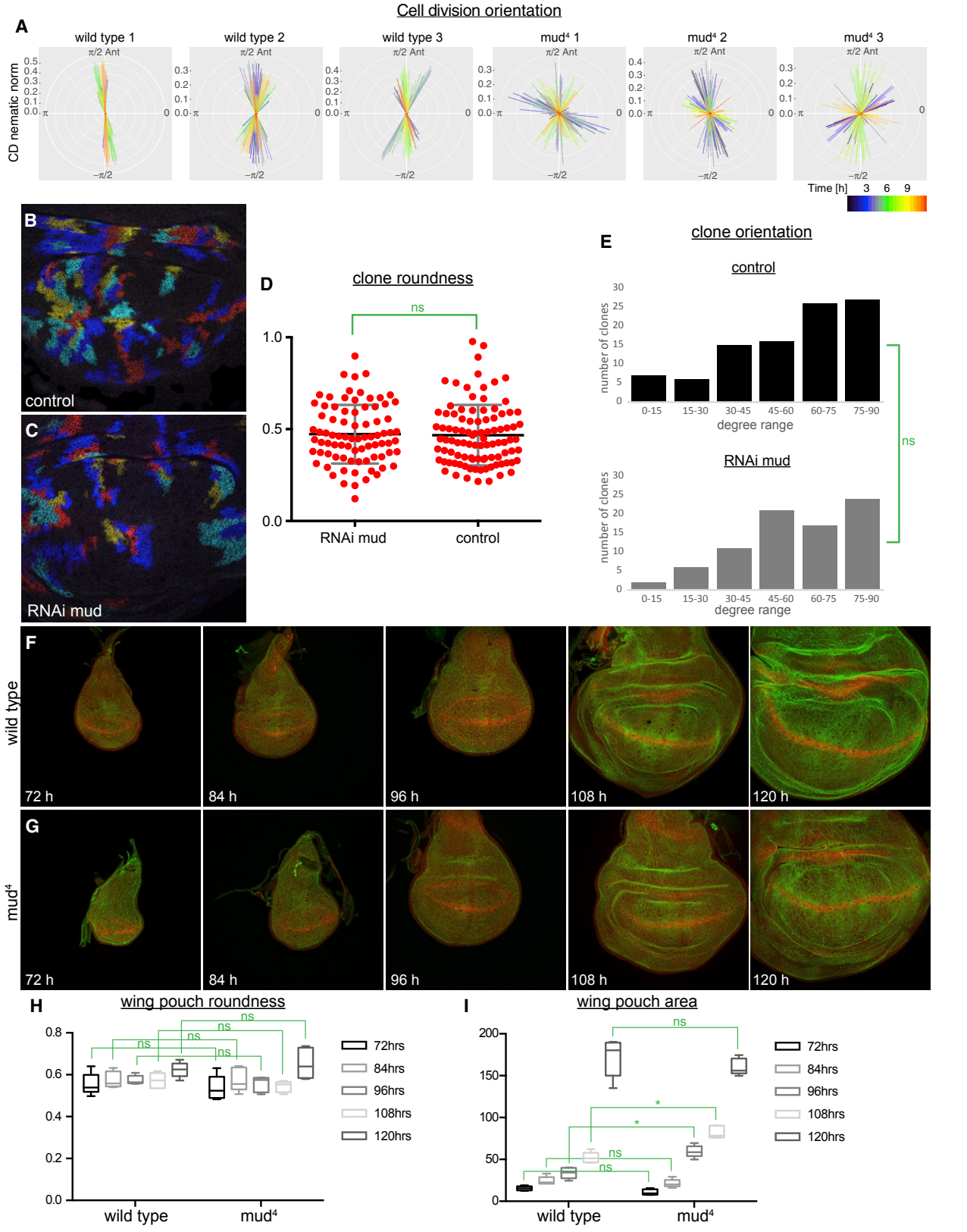

(legend on next page)

3C and S1D), although the total shear observed in *mud* mutant discs was more variable and overall less than observed in wild-type discs. As the growth of *mud* wing discs and wing pouch shape, are similar to wild-type discs *in vivo* (Figures 2F–2I), *mud* discs might be more sensitive than wild-type discs to *ex vivo* culture, but they nonetheless exhibit cell proliferation and accumulation of shear throughout *ex vivo* culture (Figure 3).

Consistent with the randomization of division orientation in *mud* mutants, cell division did not contribute significantly to the total shear observed (Figures 3 and S1). Cell elongation also contributed less to the total shear in three out of five *mud* mutant discs, which was unexpected but might suggest that randomization of spindle orientation can affect local stresses that influence cell shape. To complement our analysis of cell behaviors in culture, we also examined cell shapes and orientations in fixed discs at different times throughout third instar, and quantified the contribution of cell elongation to wing disc shape [14]. This revealed a similar overall contribution of cell elongation and orientation to wing shape between *wild-type* and *mud* mutant discs (Figure 3D). This contribution is positive (indicating a contribution of cell shape to elongation along the D-V boundary), but it declines over time [14, 19]. Our live imaging videos begin around 96 h AEL and run for 12 h. In fixed discs, we observed a greater decrease in the cell elongation contribution in wild-type discs as compared to mud^4 mutant discs from the 96- to 108-h time points, but this difference was not statistically significant (Figure 3D).

In contrast to the lack of significant contribution from cell division, T1 transitions made a substantial contribution to the total shear observed in mud^4 mutant discs and a greater contribution to disc shear than in wild-type wing discs (Figures 3C and S1D). Thus, we infer that the lack of contribution of oriented cell divisions to wing disc shear in *mud* mutant discs and to final wing shape in adult flies is compensated for at least in part by an increased contribution of T1 transitions. Although the contribution of T1 transitions to wing disc shear is greater in *mud* mutant wing discs, the total number of T1 transitions that occur is similar between wild-type and *mud* mutants (Figure 3E; Videos S3 and S4). This suggests that there is a distinct bias in the average orientation of T1 transitions in *mud* mutants as compared to wild-type wing discs.

Generation of Wing Shape

Our analysis of *mud* mutants establishes that oriented cell divisions do not make an essential contribution to normal wing morphogenesis. They occur, but they are unnecessary. Moreover, as mud^4 mutants are viable and have a normal external morphology (Figures 1F and 1G), it appears that oriented cell divisions are not required for morphogenesis of any part of the adult *Drosophila* cuticle and appendages. Suggestions that oriented cell divisions drive oriented growth hypothesize that local, individual cell behaviors (e.g., oriented cell division) are specified and then summed to determine the shape of an organ (Figure 4A). For example, in the *Drosophila* wing, it was proposed that "tissues can grow in a particular direction by controlling the orientation of cell division" [1]. Our observations instead suggest that the overall shape of the organ can be determined without specifying the cell behaviors needed to achieve it. In this view, oriented cell divisions could occur as a response to mechanisms that orient growth rather than being a cause of oriented growth.

One possible mediator of such a mechanism is mechanical stress. Cells subject to external forces can exhibit a variety of stress relaxation behaviors, including changes in cell shape, oriented divisions, and cell rearrangements [19–22]. A stress-based mechanism for wing morphogenesis could thus account for variations in the contributions of different cell behaviors to the total shear of wing discs cultured *ex vivo* [14], as well as for the continuation of normal morphogenesis when one of these mechanisms (oriented cell divisions) is abolished. Similarly, during zebrafish epiboly, tension orients cell divisions by orienting cell elongation. Epiboly can still proceed when cell division orientations are randomized but cell fusions increase [21].

Although the precise mechanism by which wing shape is specified is not yet clear, genetically, it depends upon the Dachsous-Fat pathway, as formation of rounder wings is a characteristic phenotype of mutations in genes of this pathway [23–29]. The organization of Dachsous-Fat polarity could establish tissue-wide stresses through controlling the localization of the unconventional myosin Dachs, as Dachs localization is controlled by Ds-Fat signaling [26] and Dachs can influence junctional tension [1, 30, 31]. These tissue-wide stresses could influence the overall shape of the growing wing disc and ultimately the adult wing without specifying the particular cellular behaviors by which it is achieved (Figure 4B). Consistent with this possibility, the normal proximal-distal bias in Dachs and Myosin II (Zipper, Zip) localization on junctions is maintained in *mud* mutant wing discs (Figures 4C–4F and S2).

STAR★METHODS

Detailed methods are provided in the online version of this paper and include the following:

- KEY RESOURCES TABLE
- CONTACT FOR REAGENT AND RESOURCE SHARING

Figure 2. Normally Oriented Growth in the Absence of mud

(A) Analysis of cell division nematics of three wild-type and three mud^4 live imaging videos. Different-colored lines indicate the predominant cell division orientation at different time points throughout 12 h of a live imaging video (key at bottom right).

(B and C) Examples of labeled clones (blue, cyan, red, and yellow; labeled using Raeppli technique) in wild-type (B) and *mud* RNAi (C) wing discs.

(D) Analysis of the shape of labeled clones shows a similar distribution of clone roundness in control and mud RNAi wing discs. Significance of differences calculated by t test is indicated; N = 101 clones (control) and 87 clones (mud RNAi).

(E) Analysis of the orientation of clones shows a similar bias in clone orientations perpendicular rather than parallel to the D-V boundary in control and mud RNAi wing discs. The results of chi-square tests of comparisons of the distributions are indicated; N = 97 clones (control) and 81 clones (mud RNAi).

(F and G) Images of mud^4 (G) and wild-type (F) wing discs at 72, 84, 96, 108, and 120 h AEL.

(H) The roundness of the wing pouch region (defined by Wg expression) is similar between mud^4 and wild-type at all stages.

(I) Comparison of the area of the wing pouch between mud^4 and wild-type.

Significance of differences calculated by t test is indicated; N = 5 discs for each time point of each genotype. ns, $p > 0.05$; * $p \leq 0.05$.

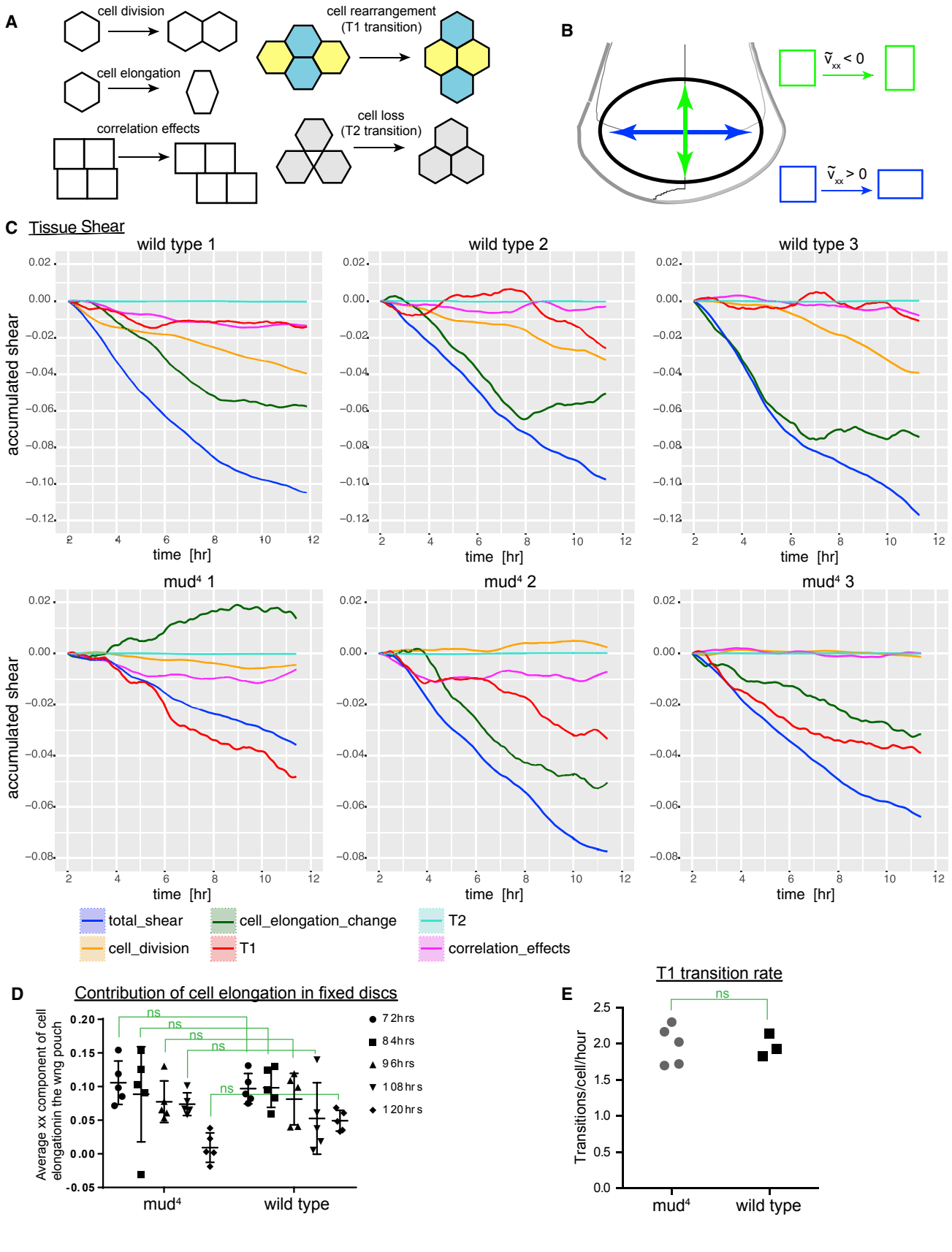

(legend on next page)

SUPPLEMENTAL INFORMATION

Supplemental Information can be found with this article online at https://doi.org/10.1016/j.cub.2019.01.044.

ACKNOWLEDGMENTS

We thank Natalie Dye and Suzanne Eaton for assistance with wing disc culture and image analysis and for helpful discussions and sharing protocols prior to publication. We thank Y. Bellaïche, the Developmental Studies Hybridoma Bank, the VDRC, and the Bloomington and Kyoto Stock Centers for antibodies and *Drosophila* stocks. We thank Shuguo Sun for establishing the Jup:RFP fly line. This research was supported by NIH grant R01 GM78620 (K.D.I.) and a Busch pre-doctoral fellowship (Z.Z.).

AUTHOR CONTRIBUTIONS

Z.Z. performed and analyzed experiments and wrote the manuscript. H.A. wrote the script for spindle orientation analysis and assisted in method development. K.D.I. supervised the research and wrote the manuscript.

DECLARATION OF INTERESTS

The authors declare no competing interests.

Received: July 16, 2018
Revised: October 21, 2018
Accepted: January 15, 2019
Published: February 21, 2019

REFERENCES

1. Mao, Y., Tournier, A.L., Bates, P.A., Gale, J.E., Tapon, N., and Thompson, B.J. (2011). Planar polarization of the atypical myosin Dachs orients cell divisions in Drosophila. Genes Dev. *25*, 131–136.
2. Baena-López, L.A., Baonza, A., and García-Bellido, A. (2005). The orientation of cell divisions determines the shape of Drosophila organs. Curr. Biol. *15*, 1640–1644.
3. Bergstralh, D.T., Dawney, N.S., and St Johnston, D. (2017). Spindle orientation: a question of complex positioning. Development *144*, 1137–1145.
4. Gillies, T.E., and Cabernard, C. (2011). Cell division orientation in animals. Curr. Biol. *21*, R599–R609.
5. LeGoff, L., and Lecuit, T. (2015). Mechanical forces and growth in animal tissues. Cold Spring Harb. Perspect. Biol. *8*, a019232.
6. Heisenberg, C.P., and Bellaïche, Y. (2013). Forces in tissue morphogenesis and patterning. Cell *153*, 948–962.
7. Li, W., Kale, A., and Baker, N.E. (2009). Oriented cell division as a response to cell death and cell competition. Curr. Biol. *19*, 1821–1826.
8. Yu, J.X., Guan, Z., and Nash, H.A. (2006). The mushroom body defect gene product is an essential component of the meiosis II spindle apparatus in Drosophila oocytes. Genetics *173*, 243–253.
9. Lu, M.S., and Johnston, C.A. (2013). Molecular pathways regulating mitotic spindle orientation in animal cells. Development *140*, 1843–1856.
10. Dewey, E.B., Sanchez, D., and Johnston, C.A. (2015). Warts phosphorylates mud to promote pins-mediated mitotic spindle orientation in Drosophila, independent of Yorkie. Curr. Biol. *25*, 2751–2762.
11. Bergstralh, D.T., Lovegrove, H.E., Kujawiak, I., Dawney, N.S., Zhu, J., Cooper, S., Zhang, R., and St Johnston, D. (2016). Pins is not required for spindle orientation in the Drosophila wing disc. Development *143*, 2573–2581.
12. Bosveld, F., Markova, O., Guirao, B., Martin, C., Wang, Z., Pierre, A., Balakireva, M., Gaugue, I., Ainslie, A., Christophorou, N., et al. (2016). Epithelial tricellular junctions act as interphase cell shape sensors to orient mitosis. Nature *530*, 495–498.
13. Karpova, N., Bobinnec, Y., Fouix, S., Huitorel, P., and Debec, A. (2006). Jupiter, a new Drosophila protein associated with microtubules. Cell Motil. Cytoskeleton *63*, 301–312.
14. Dye, N.A., Popović, M., Spannl, S., Etournay, R., Kainmüller, D., Ghosh, S., Myers, E.W., Jülicher, F., and Eaton, S. (2017). Cell dynamics underlying oriented growth of the *Drosophila* wing imaginal disc. Development *144*, 4406–4421.
15. Aigouy, B., Umetsu, D., and Eaton, S. (2016). Segmentation and quantitative analysis of epithelial tissues. Methods Mol. Biol. *1478*, 227–239.
16. Kanca, O., Caussinus, E., Denes, A.S., Percival-Smith, A., and Affolter, M. (2014). Raeppli: a whole-tissue labeling tool for live imaging of Drosophila development. Development *141*, 472–480.
17. Etournay, R., Merkel, M., Popović, M., Brandl, H., Dye, N.A., Aigouy, B., Salbreux, G., Eaton, S., and Jülicher, F. (2016). TissueMiner: a multiscale analysis toolkit to quantify how cellular processes create tissue dynamics. eLife *5*, e14334.
18. Etournay, R., Popović, M., Merkel, M., Nandi, A., Blasse, C., Aigouy, B., Brandl, H., Myers, G., Salbreux, G., Jülicher, F., and Eaton, S. (2015). Interplay of cell dynamics and epithelial tension during morphogenesis of the Drosophila pupal wing. eLife *4*, e07090.
19. Mao, Y., Tournier, A.L., Hoppe, A., Kester, L., Thompson, B.J., and Tapon, N. (2013). Differential proliferation rates generate patterns of mechanical tension that orient tissue growth. EMBO J. *32*, 2790–2803.
20. Wyatt, T.P.J., Harris, A.R., Lam, M., Cheng, Q., Bellis, J., Dimitracopoulos, A., Kabla, A.J., Charras, G.T., and Baum, B. (2015). Emergence of homeostatic epithelial packing and stress dissipation through divisions oriented along the long cell axis. Proc. Natl. Acad. Sci. USA *112*, 5726–5731.
21. Campinho, P., Behrndt, M., Ranft, J., Risler, T., Minc, N., and Heisenberg, C.-P. (2013). Tension-oriented cell divisions limit anisotropic tissue tension

Figure 3. Cellular Components of Tissue Shear in *mud* Mutants

(A) Illustrations of different types of cell dynamics that can contribute to tissue shear [17, 18].

(B) Schematic illustrating how the sign of the shear tensor indicates the direction of the change in shape.

(C) Analysis of accumulated shear (blue) and the contribution of different cellular processes to this shear (key at bottom) in three wild-type and three mud^4 discs from 2–12 h of culture, averaged over the entire tracked region.

(D) Analysis of the xx component of cell elongation, averaged throughout the wing pouch of mud^4 and wild-type wing discs at 72, 84, 96, 108, and 120 h AEL that were imaged as illustrated in Figure 2 and then segmented based on E-cadherin:GFP to outline all cells. Each dot represents the averaged value for one disc; center line indicates the mean value. Significance of differences calculated by t test is indicated; N = 5 discs for each time point of each genotype.

(E) Scatterplot showing the T1 transition rates within segmented videos of wild-type and mud^4 *ex vivo* culture. Significance of difference calculated by t test is indicated.

ns, $P > 0.05$. See also Figure S1 and Videos S1, S2, S3, and S4.

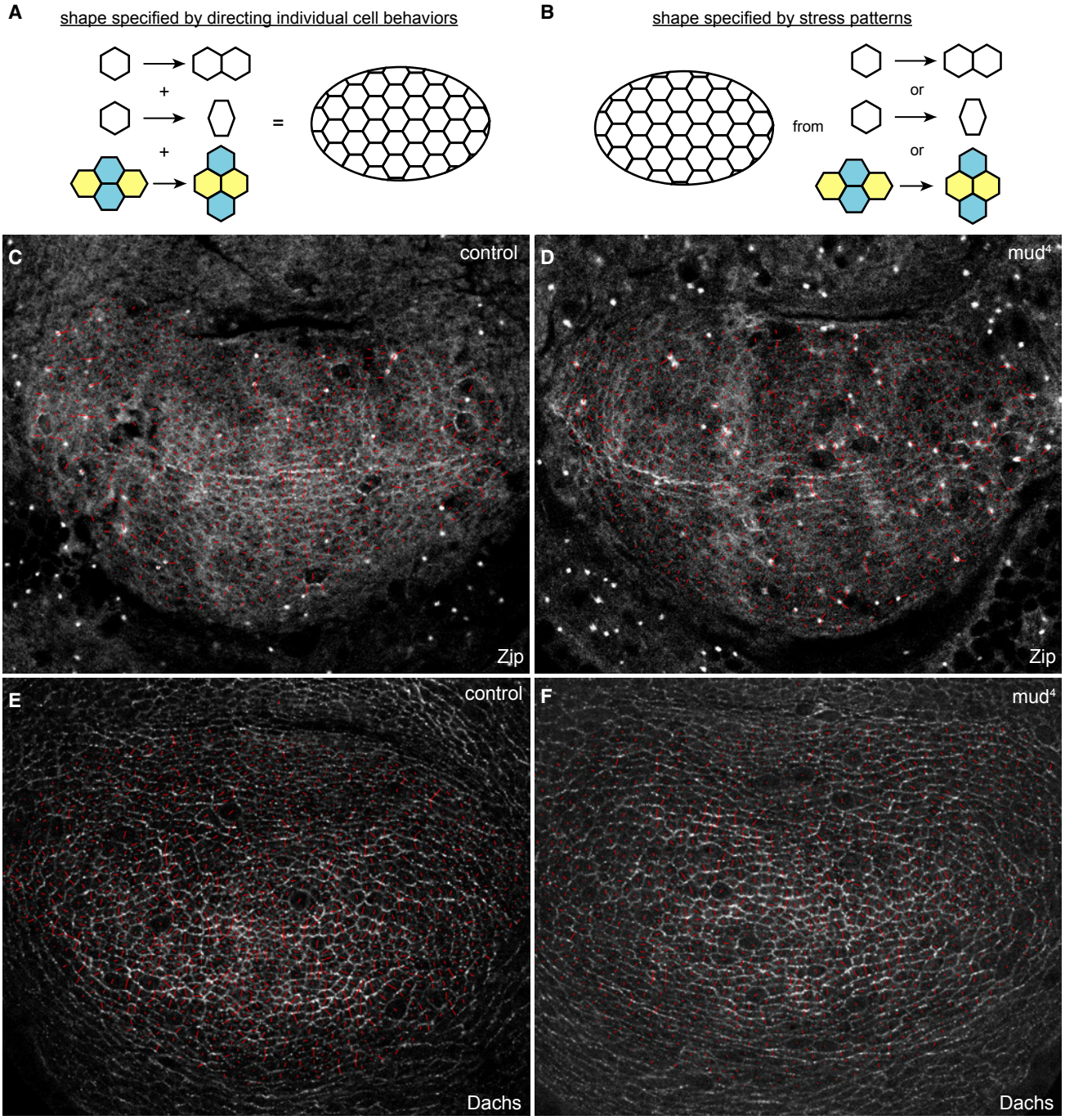

Figure 4. Relating Cell Behaviors to Wing Shape

(A and B) Cartoons illustrating two alternative mechanisms for controlling morphogenesis.

(A) Organ shape is generated by specifying and then summing individual cell behaviors.

(B) Organ shape is generated by defining a "morphogenetic space" that can be filled through a variety of cell behaviors, whose contributions are not individually defined and may vary in different animals.

(C–F) Examples of wing discs expressing GFP-tagged Myosin II heavy chain (Zip; C and D) or Dachs (E and F) in wild-type control (C and E) or *mud*^{4} mutant (D and F) males. Red lines superimposed on the images indicate anisotropy of junctional Zip or Dachs within each cell, with the orientation indicating the axis of anisotropy and the length indicating the magnitude of anisotropy.

See also Figure S2.

in epithelial spreading during zebrafish epiboly. Nat. Cell Biol. *15*, 1405–1414.

22. Aegerter-Wilmsen, T., Smith, A.C., Christen, A.J., Aegerter, C.M., Hafen, E., and Basler, K. (2010). Exploring the effects of mechanical feedback on epithelial topology. Development *137*, 499–506.
23. Misra, J.R., and Irvine, K.D. (2016). Vamana couples Fat signaling to the Hippo pathway. Dev. Cell *39*, 254–266.
24. Mao, Y., Kucuk, B., and Irvine, K.D. (2009). Drosophila lowfat, a novel modulator of Fat signaling. Development *136*, 3223–3233.
25. Matakatsu, H., and Blair, S.S. (2008). The DHHC palmitoyltransferase approximated regulates Fat signaling and Dachs localization and activity. Curr. Biol. *18*, 1390–1395.
26. Mao, Y., Rauskolb, C., Cho, E., Hu, W.L., Hayter, H., Minihan, G., Katz, F.N., and Irvine, K.D. (2006). Dachs: an unconventional myosin that functions downstream of Fat to regulate growth, affinity and gene expression in Drosophila. Development *133*, 2539–2551.
27. Villano, J.L., and Katz, F.N. (1995). four-jointed is required for intermediate growth in the proximal-distal axis in Drosophila. Development *121*, 2767–2777.
28. Clark, H.F., Brentrup, D., Schneitz, K., Bieber, A., Goodman, C., and Noll, M. (1995). Dachsous encodes a member of the cadherin superfamily that controls imaginal disc morphogenesis in Drosophila. Genes Dev. *9*, 1530–1542.
29. Mahoney, P.A., Weber, U., Onofrechuk, P., Biessmann, H., Bryant, P.J., and Goodman, C.S. (1991). The fat tumor suppressor gene in Drosophila encodes a novel member of the cadherin gene superfamily. Cell *67*, 853–868.
30. Bosveld, F., Bonnet, I., Guirao, B., Tlili, S., Wang, Z., Petitalot, A., Marchand, R., Bardet, P.L., Marcq, P., Graner, F., and Bellaïche, Y. (2012). Mechanical control of morphogenesis by Fat/Dachsous/Four-jointed planar cell polarity pathway. Science *336*, 724–727.
31. Bosveld, F., Guirao, B., Wang, Z., Rivière, M., Bonnet, I., Graner, F., and Bellaïche, Y. (2016). Modulation of junction tension by tumor suppressors and proto-oncogenes regulates cell-cell contacts. Development *143*, 623–634.
32. Oda, H., and Tsukita, S. (2001). Real-time imaging of cell-cell adherens junctions reveals that Drosophila mesoderm invagination begins with two phases of apical constriction of cells. J. Cell Sci. *114*, 493–501.
33. Rauskolb, C., Pan, G., Reddy, B.V., Oh, H., and Irvine, K.D. (2011). Zyxin links fat signaling to the hippo pathway. PLoS Biol. *9*, e1000624.
34. Schindelin, J., Arganda-Carreras, I., Frise, E., Kaynig, V., Longair, M., Pietzsch, T., Preibisch, S., Rueden, C., Saalfeld, S., Schmid, B., et al. (2012). Fiji: an open-source platform for biological-image analysis. Nat. Methods *9*, 676–682.
35. Heemskerk, I., and Streichan, S.J. (2015). Tissue cartography: compressing bio-image data by dimensional reduction. Nat. Methods *12*, 1139–1142.
36. Sommer, C., Straehle, C., Köthe, U., and Hamprecht, F.A. (2011). ilastik: interactive learning and segmentation toolkit. In 2011 IEEE International Symposium on Biomedical Imaging: From Nano to Macro (IEEE).
37. R Core Team (2016). R: a language and environment for statistical computing. http://www.r-project.org/.
38. Aigouy, B., Farhadifar, R., Staple, D.B., Sagner, A., Röper, J.-C., Jülicher, F., and Eaton, S. (2010). Cell flow reorients the axis of planar polarity in the wing epithelium of Drosophila. Cell *142*, 773–786.
39. Venken, K.J., Schulze, K.L., Haelterman, N.A., Pan, H., He, Y., Evans-Holm, M., Carlson, J.W., Levis, R.W., Spradling, A.C., Hoskins, R.A., and Bellen, H.J. (2011). MiMIC: a highly versatile transposon insertion resource for engineering Drosophila melanogaster genes. Nat. Methods *8*, 737–743.

STAR★METHODS

KEY RESOURCES TABLE

REAGENT or RESOURCE	SOURCE	IDENTIFIER
Antibodies		
Anti-wingless	DSHB	RRID: AB_528512
Anti-Cleaved Caspase	Cell Signaling	RRID: AB_2721060
Anti-E-cad	DSHB	RRID: AB_528120
Chemicals, Peptides, and Recombinant Proteins		
Paraformaldehyde	Fisher Scientific	Cat# T353-500
Hoechst	Invitrogen	Cat# H3570
Grace's Insect Medium	Sigma-Aldrich	Cat# G9771
20-hydroxyecdysone	Sigma-Aldrich	Cat# H5142-5MG
BisTris	Sigma-Aldrich	Cat# B4429-25G
Fetal Bovine Serum	Thermo-Fisher	Cat# 10082147
Pen Strep	Thermo-Fisher	Cat# 15070063
Experimental Models: Organisms/Strains		
Fly: Ubi-Ecad:GFP	[32]	N/A
Fly: Jupiter:RFP	This manuscript	N/A
Fly: zip:GFP	BDSC	Stock# 51564
Fly: dachs:GFP	[31]	N/A
Fly: *mud*^{4}/*FM7i*	BDSC	Stock# 9563
Fly: UAS-RNAi mud	BDSC	Stock# 38190
Fly: w;P(w[+mC] = Raeppli-CAAX)67E	BDSC	Stock# 55083
Fly: nubbin-Gal4 UAS-dcr2	[33]	N/A
Software and Algorithms		
Matlab2016b	Mathworks	http://mathworks.com
Fiji	[34]	https://fiji.sc
ImSAnE MATLAB script	[35]	https://media.nature.com/original/nature-assets/nmeth/journal/v12/n12/extref/nmeth.3648-S2.zip
ilastik	[36]	http://ilastik.org/index.html
Prism 6.0	GraphPad	https://www.graphpad.com/scientific-software/ prism/, RRID: SCR_002798
R ver.3.4.1	[37]	https://www.r-project.org
TissueAnalyzer	[38]	https://grr.gred-clermont.fr/labmirouse/software/WebPA/index.html
TIssueMiner	[17]	https://github.com/mpicbg-scicomp/tissue_miner
Spindle Orientation script	This manuscript	https://github.com/alegoth/Spindle-Orientation-Analysis
Others		
35mm Petri dish	MatTek corporation	P35G-0-14-C
Cyclopore polycarbonate membrane	GE healthcare	Cat# 7060-2513
Leica SP8 confocal	Leica Microsystems	https://www.leica-microsystems.com/
UltraView Spinning disc confocal	PerkinElmer	http://www.perkinelmer.com/lab-products-and-services/cellular-imaging/confocal-imaging.html

CONTACT FOR REAGENT AND RESOURCE SHARING

Further information and requests for reagents may be directed to and will be fulfilled by the Lead Contact Kenneth D. Irvine (irvine@waksman.rutgers.edu).

EXPERIMENTAL MODEL AND SUBJECT DETAILS

Unless otherwise indicated, flies were raised on standard medium at 25°C. w^{1118} are used as control flies. Ubi-Ecad:GFP was obtained from the Kyoto stock center. Jupitor:RFP was created from the MiMIC line Jupiter^{MI00919} by insertion of the TagRFP 3xHA cassette [39] using services of BestGene. P(w[+mC] = Raeppli-CAAX)67E/TM6B for Reappli and other flies were obtained from the Bloomington *Drosophila* stock center. Both male and female flies were used. For measurements of wing area, males and females were analyzed separately at 1 day after eclosion. The information for all fly lines is described in the Key Resources Table.

METHOD DETAILS

Quantification of adult wings

Adult wing phenotypes of *mud* mutants were scored by comparing mud^4 hemizygous and w^{1118} males. Adult wing phenotypes of *mud* RNAi were scored by crossing *nub-Gal4 UAS-dcr2* females to *UAS-RNAi mud /CyO,GFP* or *If/CyO,GFP* (control) males. All wings were photographed at the same magnification. For quantification, at least 12 wings per genotype were manually traced in Fiji (NIH ImageJ) and then analyzed using area and shape descriptors measure functions of Fiji. This calculates roundness using 4 x Area/(π x [Major axis]^2).

Examination and quantitation of fixed wing discs

y w; Ubi-Ecad:GFP/CyO,GFP; Jupitor:RFP/TM6B males were crossed with either mud^4 or w^{1118} females. Wing discs from male larvae at specified time points after egg laying (AEL) were dissected and fixed in 4% paraformaldehyde (Fisher, T353-500) for 12 min at room temperature, and stained using mouse anti-Wg (1:400, DSHB) and donkey anti-mouse IgG:Cy5 (Jackson ImmunoResearch). Wing discs were mounted on a microscope slide and images captured on a Leica SP8 confocal microscope.

The wing pouch was defined by anti-Wg staining, and quantified by manually tracing this region in Fiji, and calaculating the area and roundness using the Area and Shape descriptors measurement functions of Fiji.

For cell elongation analysis, the E-cad:GFP channel from confocal images of fixed wing discs were processed with the ImSAnE MATLAB script [35] to project the apical plane onto a 2D surface based on maximal brightness of the E-Cadherin-GFP signal. The E-cad signal in the central pouch region was then segmented using Tissue Analyzer. Tissue Miner was then used to plot the xx component of cell elongation averaged by the area for each disc and the results were plotted using Graphpad Prism software.

Quantification of Zip and Dachs anisotropy

zip:GFP or *dachs:GFP* males were crossed with either mud^4 or w^{1118} females. Wing discs from male larvae at 96 h AEL were dissected and fixed in 4% paraformaldehyde (Fisher, T353-500) for 12 min at room temperature, and stained using rat anti-E-cad (1:400, DSHB) and donkey anti-rat IgG:Cy5 (Jackson ImmunoResearch). Wing discs were mounted on a microscope slide and images captured on a Leica SP8 confocal microscope. For quantification of protein anisotropy, confocal image stacks were first processed with the ImSAnE MATLAB script to project the apical surface onto a 2D plane based on maximal brightness of the E-Cad. Cells were then segmented based on E-Cad staining and the anisotropy of Zip:GFP or Dachs:GFP for each cell was characterized using TissueAnalyzer software.

Quantification of Raeppli clones

Raeppli clones were generated by crossing y w; nub-Gal4 UAS-dcr2/CyO,GFP; P(w[+mC] = Raeppli-CAAX)67E/TM6B females to either y w hs-Flp;UAS-RNAi-mud/CyO,GFP; Ubi-Ecad:GFP/TM6B or y w hs-Flp ;If/CyO,GFP; Ubi-Ecad:GFP/TM6B (control) males for 4 h and then maintaining them at 29°C. Larvae were heat shocked at 90 h AEL and dissected at 120 h AEL. To quantify clone shape and orientation, clone boundaries were traced manually and measured using the Shape descriptors functions of Fiji.

Live imaging and analysis of wing discs cultured *ex vivo*

For live imaging of *mud* mutants, *y w; Ubi-Ecad:GFP/CyO,GFP; Jupitor:RFP/TM6B* male flies were crossed with either mud^4 or w^{1118} (control) females and then male larval progeny were examined. For live imaging of *mud* RNAi knock-down, *nub-Gal4 UAS-dcr2 / CyO,GFP; Ubi-Ecad:GFP/TM6B* females were crossed to either *UAS-RNAi mud /CyO,GFP;* Jupitor:RFP/TM6B or *If/CyO,GFP; Jupitor:RFP/TM6B* (control) males. Wing disc culture was based on the procedure of Dye et al. [14]. A stock medium was prepared using Grace's medium (Sigma, G9771) without sodium bicarbonate but with the addition of 5mM Bis-Tris and the pH was adjusted to 6.6-6.7 at room temperature. This was stored at 4°C for less than a month. Before every experiment, we added 5% fetal bovine serum (FBS; ThermoFisher, 10082147), Penicillin-Streptomycin (Thermo-Fisher, #15070063, 100 × stock solution) and 10 nM 20-hydroxyecdysone (Sigma, H5142) to the medium. Larvae at 96h AEL were floated on 25% sucrose and transferred into glass dishes with culture medium. Larvae of the desired genotype were selected and sterilized in 70% ethanol for 1-2 mins. We then drew a circle on the glass bottom of a 35-mm glass-bottomed Petri dish (MatTek, P35G-0-14-C) using glue from tape (Tesa, 5388). Wing discs were dissected out of larvae and transferred into this Petri dish. Then we covered the discs with cyclopore polycarbonate membrane (GE health, 7060-2513) and glued it to the glass bottom to immobilize discs. Live wing discs were then imaged using a Perkin Elmer Ultraview spinning disc confocal microscope every 6-8 mins for 12 hours.

For analysis of spindle orientation, the Jupiter:RFP channel was segmented using Ilastik. Spindle orientation was determined using a custom MATLAB script, when the spindles merge into one spindle line, which occurs after spindle rotations have completed. The orientations of spindles relative to the D-V boundary were calculated using Excel.

For analysis of tissue shear and its component cellular contributions, confocal image stacks were first processed with the ImSAnE MATLAB script to project the apical surface onto a 2D plane based on maximal brightness of the E-Cadherin-GFP signal. Segmentation and cell tracking was then performed on the central wing pouch of the projected time lapse images using Tissue Analyzer. Manual correction of segmentation was required for every time frame of each video, which typically takes 2 weeks per video. Analysis of tissue shear and its cellular contributions was calculated using Tissue Miner.

QUANTIFICATION AND STATISTICAL ANALYSIS

For quantification of adult wings, at least 12 wings per genotype were manually traced in Fiji (NIH ImageJ) and then analyzed using area and shape descriptors measure functions of Fiji. Statistical significance of pairwise comparisons was assessed by t test using Prism 7 software (GraphPad). For quantification of fixed wing discs, the wing pouch was defined by anti-Wg staining, and quantified by manually tracing this region in Fiji, and calculating the area and roundness using the Area and Shape descriptors measurement functions of Fiji. Statistical significance of pairwise comparisons for each time point was assessed by t test using Prism 7 software (GraphPad). For quantification of Zip and Dachs anisotropy, the anisotropy of Zip:GFP or Dachs:GFP for each cell was characterized using TissueAnalyzer software. Statistical analysis was performed using Chi square in R (ver.3.4.1) with R stats package. To quantify Reappli clone shape and orientation, clone boundaries were traced manually and measured using the Shape descriptors functions of Fiji. Statistical significance of pairwise comparisons was assessed by t test using Prism 7 software (GraphPad). For quantification of spindle orientation, the orientations of spindles relative to the D-V boundary were calculated using a custom MATLAB script. Statistical analysis was performed using Chi square in R (ver.3.4.1) with R stats package. For each dataset, details of n-values can be found in the corresponding figure legends.

DATA AND SOFTWARE AVAILABILITY

A custom MATLAB script was used to determine the final orientation of mitotic spindles in live imaging videos based on segmentation of the Jup:RFP stain. This script is available at https://github.com/alegoth/Spindle-Orientation-Analysis

Current Biology, Volume *29*

Supplemental Information

Oriented Cell Divisions Are Not Required for *Drosophila* Wing Shape

Zhenru Zhou, Herve Alégot, and Kenneth D. Irvine

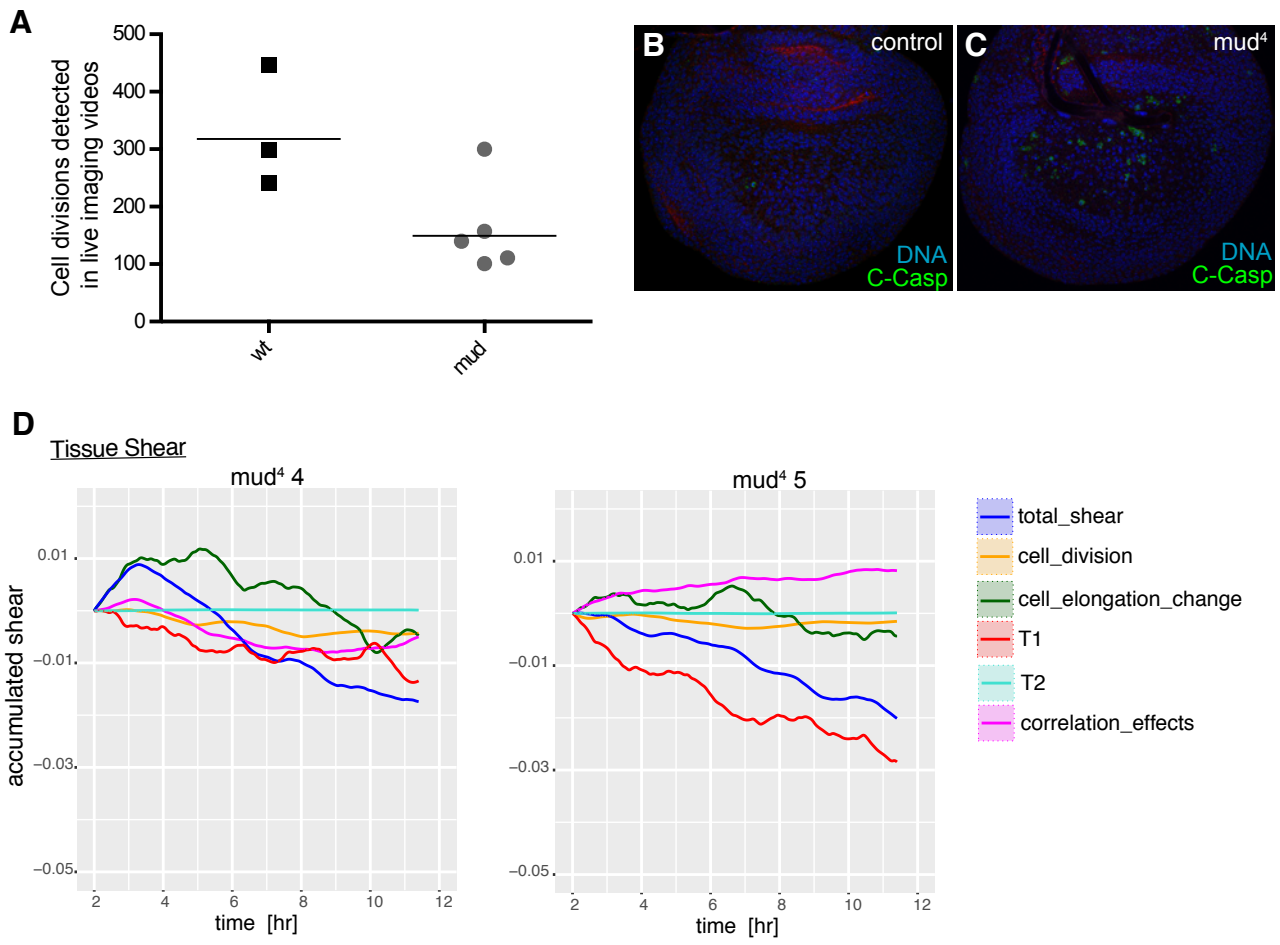

Figure S1. Additional analysis of cell behavior in wing discs, related to Figure 3

A) Scatter plot showing the number of cell divisions detected based on segmentation of cell junctions over 12h of ex vivo culture in three wild-type and five mud mutant videos. B,C) Examples of wing discs from wild-type control (B) and mud mutant (C) wing discs, stained for DNA (blue) and cleaved caspase (green). (D) Analysis of accumulated shear (blue) and the contribution of different cellular processes to this shear (key at bottom) in two additional mud4 discs from 2 - 12 h of culture, averaged over the entire tracked region.

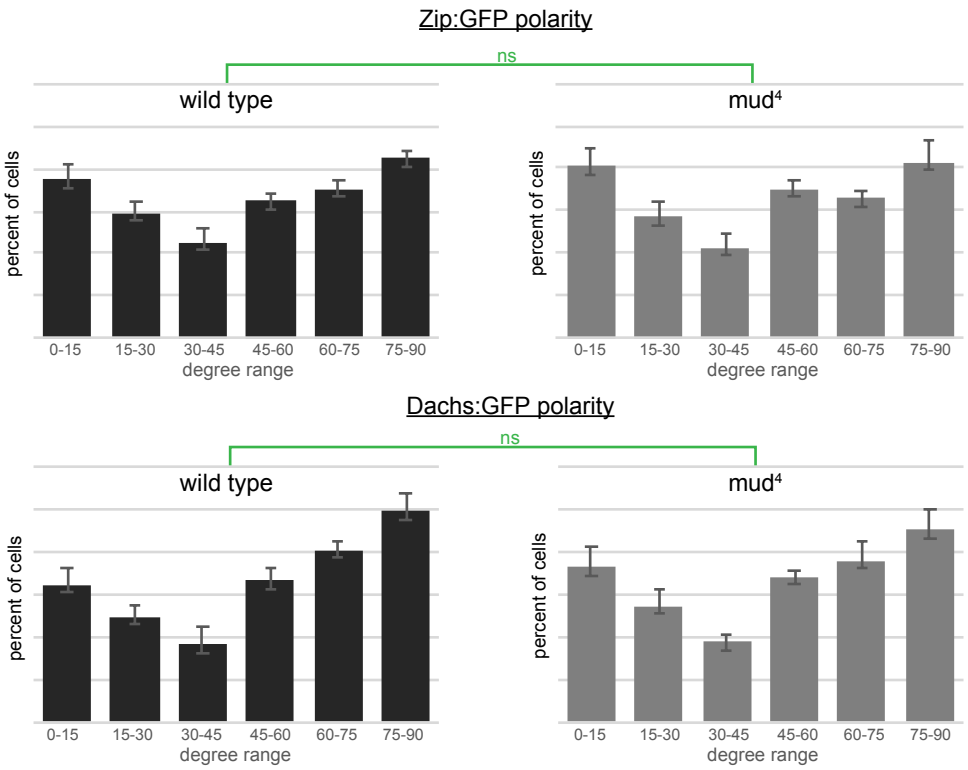

Figure S2. Analysis of Zip and Dachs polarity, related to Figure 4
Quantitation of the polarity vectors for Zip:GFP and Dachs:GFP in individual cells, binned into 15 degree increments relative to the D-V boundary, from five discs per genotype, with 7000-10,000 cells analyzed per genotype. Error bars indicate standard deviation between discs. Greens bars indicate the results of Chi square analysis.